3D Hydrophobic Moment Vectors as a Tool to Characterize the Surface Polarity of Amphiphilic Peptides

Sabine Reißer,[†‡] Erik Strandberg,[†] Thomas Steinbrecher,[‡*] and Anne S. Ulrich[†§*]

[†]Institute of Biological Interfaces II, [‡]Institute of Physical Chemistry, and [§]Institute of Organic Chemistry, Karlsruhe Institute of Technology, Karlsruhe, Germany

ABSTRACT   The interaction of membranes with peptides and proteins is largely determined by their amphiphilic character. Hydrophobic moments of helical segments are commonly derived from their two-dimensional helical wheel projections, and the same is true for β-sheets. However, to the best of our knowledge, there exists no method to describe structures in three dimensions or molecules with irregular shape. Here, we define the hydrophobic moment of a molecule as a vector in three dimensions by evaluating the surface distribution of all hydrophilic and lipophilic regions over any given shape. The electrostatic potential on the molecular surface is calculated based on the atomic point charges. The resulting hydrophobic moment vector is specific for the instantaneous conformation, and it takes into account all structural characteristics of the molecule, e.g., partial unfolding, bending, and side-chain torsion angles. Extended all-atom molecular dynamics simulations are then used to calculate the equilibrium hydrophobic moments for two antimicrobial peptides, gramicidin S and PGLa, under different conditions. We show that their effective hydrophobic moment vectors reflect the distribution of polar and nonpolar patches on the molecular surface and the calculated electrostatic surface potential. A comparison of simulations in solution and in lipid membranes shows how the peptides undergo internal conformational rearrangement upon binding to the bilayer surface. A good correlation with solid-state NMR data indicates that the hydrophobic moment vector can be used to predict the membrane binding geometry of peptides. This method is available as a web application on http://www.ibg.kit.edu/HM/.

INTRODUCTION

Understanding the mechanism of interaction between amphiphilic peptides and membranes is a central goal of many investigations on antimicrobial agents, cell-penetrating carriers, and peripheral membrane proteins in general (1–9). For example, membrane binding is the first step in the formation of peptidic transmembrane pores, and further transitions between surface-bound and inserted structures are often of functional significance (10–13). The structural information of helical membrane-bound peptides is typically described in an internal coordinate system defined by the helix tilt angle, azimuthal rotation angle, and insertion depth, and by whole-body dynamics (14–18). Structural information is accessible from solid-state NMR experiments in oriented membrane samples (19–23) using, for example, ^{2}H-, ^{15}N-, or ^{19}F-NMR (17,18,24–51). In addition, information about the tilt angle of α-helices can be obtained by oriented circular dichroism (29,52–57). In recent years, both coarse-grained and all-atom molecular dynamics (MD) simulations have been used to reproduce and predict the geometry of peptide-membrane assemblies (2,58–62). The use of MD methods for structure prediction requires analysis tools that condense large amounts of simulation data into experimentally verifiable values.

In this work, we have defined and utilized three-dimensional (3D) hydrophobic moment (HM) vectors as a to our knowledge new tool for predicting peptide-bilayer binding geometries. This 3D approach extends the idea of molecular hydrophobicity potentials (MHPs), which are based on heuristic (63) or experimental (64–68) definitions of hydrophobicity for whole residues (65), molecular fragments, or individual atoms (69). Tools like Membrane Protein Explorer (Stephen White Laboratory, University of California, Irvine, CA) (70) use these hydrophobicity scales to calculate water-bilayer transfer energies for small peptides. The first concept of an HM for individual protein helices was presented in 1982 by Eisenberg et al. (71,72). Based on their experimentally determined amino acid side-chain hydrophobicities (72), a two-dimensional (2D) HM vector is calculated that represents the distribution of hydrophobic and hydrophilic residues perpendicular to the helix axis. In this way, it is possible to categorize helical peptides according to their amphiphilicity and to roughly predict the geometry of their insertion into a membrane. More recently, refined hydrophobicity scales have been developed (73), and that methodology is used regularly for the analysis of membrane proteins (74). The Eisenberg definition of a 2D HM vector is useful for a qualitative description of peptide helices, but it is limited in its applicability to structures of close-to-ideal α-helical geometry. Amphiphilic gradients along the helix axis cannot be taken into consideration either, because the calculation relies on a projection of the vector onto the plane of the helical wheel. Furthermore, the commonly used hydrophobicity scales have been determined with respect to the free energies of transferring isolated amino acid side chains from polar to nonpolar

CrossMark

environments (72). These scales do not take into account the cooperativity between side chains (e.g., salt bridges), nor any conformational rearrangements within a whole peptide (e.g., upon membrane binding).

To establish a simple, and generally applicable, method to compute 3D HMs for arbitrary molecules, we combine structural data from MD simulations according to the protocol outlined below. It is based on the electrostatic potential on the peptide surface, computed via Poisson-Boltzmann continuum electrostatics calculations. We show here, for two representative peptides of different conformation, size, and hydrophobicity, that their 3D HM vectors align with the membrane normal. We have selected a pair of structurally different, well-characterized antimicrobial peptides (AMPs)—PGLa (11,30,39,41,46,47,51,52,75–79) and the cyclic β-pleated gramicidin S (48,49,80–82)—as a test set. For the latter peptide, the currently established methods for HM calculation are not applicable. Both of these peptides are found to undergo conformational changes upon membrane binding, so that their HM vectors increase and their interactions with the lipid bilayer are optimized.

METHODS

All MD simulations were conducted using the molecular simulation package GROMACS 4.5.5 (83). As model systems, we selected two antimicrobial peptides: the cyclic decapeptide gramicidin S (GS, charge $+2$, *cyclo* [PVOL-^{D}F]$_2$, where O stands for ornithine) (48,49,80–82) and the helical 21-mer PGLa (charge $+5$, GMASKAGAIAGKIAKVALKAL-NH$_2$) (11,30,39,41,46,47,51,52,75–78), which we have studied extensively in the past. Simulations were conducted in methanol or water for solvated conditions, and in a dimyristoylphosphatidylcholine (DMPC) bilayer for the membrane-bound states. The water model was TIP3P, and AMBER99 parameters were used for methanol. For the peptide/lipid systems, the AMBER99SB-ILDN (84) force field was used with the SLIPID force field for the lipids (85). The starting conformation for gramicidin S was constructed using the xleap tool from the AmberTools modeling suite (86), based on dihedral angles obtained from a high-resolution liquid-state NMR structure (87). PGLa was modeled as an ideal α-helix, based on helicity measurements by CD spectroscopy (47). The peptide-membrane complexes were constructed by conducting unrestrained membrane binding simulations 10 ns in length, by placing the peptide molecules parallel to preequilibrated lipid bilayers at distances of 2–4 nm from each other, at an elevated temperature of 480 K to speed up insertion. During the high-temperature insertion, hydrogen bonds in PGLa were restrained using distance restraints of 1000 kJ/(mol nm^2) to prevent unfolding. After cooling down to 303 K, a short equilibration run of 500 ps with position restraints of 1000 kJ/(mol nm^2) on the membrane-inserted peptides was performed to allow temperature and volume to stabilize. Then, the systems were simulated without any restraints at 303 K for another 650/600 ns (gramicidin S/PGLa) in the NPT ensemble, until converged structural ensembles were obtained (see RMSD plots in Figs. S1–S4 in the Supporting Material). Unrestrained production simulations were conducted using a Nosé-Hoover thermostat (88) and Parrinello-Rahman barostat (89), with semiisotropic pressure coupling in the case of lipid bilayer systems. A time step of 2 fs was used for all simulations, together with the LINCS algorithm (90) to constrain bonds involving hydrogen atoms. Long-range electrostatics were treated via particle mesh Ewald combined with a 1.4 nm direct-space cutoff for van der Waals and Coulomb interactions.

Gramicidin S was simulated for 600 ns at 303 K embedded in a box of ~1000 methanol molecules, and for 650 ns in a lipid bilayer composed of

72 preequilibrated DMPC molecules solvated with ~2000 TIP3P water molecules and chloride counterions. PGLa was simulated for 600 ns at 303 K in solution in a box with ~6000 water molecules and chloride counterions, and for 600 ns embedded in a preequilibrated bilayer composed of 100 DMPC lipid molecules solvated with ~3000 TIP3P water molecules and chloride counterions. For each peptide-membrane system, two or three control simulations were performed, each 400 ns in length and according to the same protocol, but with slightly different peptide starting positions.

The last 100 ns of each simulation were used to compute and analyze the HM based on 100 structural snapshots collected at equidistant time steps of 1 ns. In addition, to determine the averaging procedure, we performed the calculation on one of the PGLa simulations at a smaller time step of 50 ps so that we would have 20 times more snapshots, and over the last 300 ns instead of over the last 100 ns. All of these different data sets (100, 2000, 300, and 6000 snapshots) gave almost the same average values for the HM vector, the maximal difference being 1.2% (see Table S1; also, Fig. S5 describes the evolution of the different properties). Considering the fast fluctuations of the values and the considerable amount of calculation time needed (~1 min/snapshot), we find that a choice of 100 snapshots taken at time steps of 1 ns for 100 ns of equilibrated trajectory is justified.

Solvent and lipid molecules were removed, and continuum solvent calculations were set up for the peptides using PARSE radii (91), whereas atomic partial charges were kept from the force field.

For each structure, the solvent-accessible surface was calculated as a set of discrete triangles using NanoShaper (92). The APBS (93) numerical Poisson-Boltzmann solver was used to compute the electrostatic potential, V_e, on every surface-triangle vertex. The interior dielectric constant for the peptide solutes was set to 2.0 to account for electronic polarization effects. Solvent dielectric constants of 78.5 were used for an aqueous environment, of 32.6 for methanol solvation, and of 20.0 for the membrane-water interface as an interpolation between the polar aqueous and hydrophobic bilayer interior conditions. Based on the continuum electrostatic calculations, we define the resulting HM vector, $\vec{\mu}$, as

$$\vec{\mu} = \sum_{i=1}^{n} \sum_{j=1}^{3} \left(\langle |V_e| \rangle - |V_e|_{ij} \right) \times \vec{r}_{ij}. \tag{1}$$

The sum over i runs over all triangles, and the sum over j runs over the three corner points of each triangle. $|V_e|_{ij}$ is the absolute value of the electric potential at the corner point labeled ij. All parts of the surface that have an absolute electric potential, $|V_e|$, greater than the average absolute potential are counted as negative or polar, whereas the parts with lower-than-average electric potential are counted as positive or unpolar. The average absolute potential $\langle |V_e| \rangle$ is defined as

$$\langle |V_e| \rangle = \frac{1}{A_{tot}} \sum_{i=1}^{n} \sum_{j=1}^{3} |V_e|_{ij} \times \frac{A_i}{3}. \tag{2}$$

Due to the uneven spacing of the triangulated surface, the potential on each vertex is scaled by one-third of the area of the surrounding triangles, A_i. The whole sum is then divided by the total surface area, A_{tot}. The vector $\vec{r}_{ij}$ in Eq. 1 points toward the vertex ij and is defined as

$$\vec{r}_{ij} = \vec{x}_{ij} \times \frac{A_i}{3 \times A_{tot}}, \tag{3}$$

where $\vec{x}_{ij}$ is the actual vertex vector. As above, $\vec{x}_{ij}$ is scaled by one-third of the surrounding triangle area. This way, we avoid an overestimation of highly curved parts of the surface that contain a lot of vertices.

A_{tot} is simply the sum over all triangles:

$$A_{tot} = \sum_{i=1}^{n} A_i. \tag{4}$$

We use absolute values for the electrostatic potential, since we aim to describe the differential distribution of polar and unpolar patches on the surface, effectively constructing a vector, $\vec{\mu}$, that points away from the most polar parts of the molecular surface. By using the difference between the absolute surface potential at each point and the average absolute surface potential, $\vec{\mu}$ reflects the distribution of polar patches on the surface (not the total polarity of the molecule).

If the electrostatic potential is given in kT/e and the vectors in Ångströms, the resulting HM vector has a unit of 2.56×10^{-12} Vm at room temperature. Since this unit doesn't carry any physical implication, we omit it in the following discussion and give $\vec{\mu}$ in multiples of kTÅ/e.

For each set of 100 snapshots, we calculated the average HM vector, the average angular variation from the average vector, and the standard deviation of the vector length. For simulations in the membrane, the angle between the average HM vector and the membrane normal was calculated as well. The VMD software (94) was used to visualize the results.

RESULTS

Model charge distributions

To illustrate the principle and to help visualize the results obtained from HM calculations, we created a model system consisting of a hexagonal pseudomolecule shaped like benzene, on which we placed varying charge distributions (Fig. 1). In the initial form, all partial charges were set to zero, and various sets of 1–4 positive and/or negative charges, each of magnitude 0.3e, were distributed around the ring.

The trivial situations of no charge or a single charge result in no HM or an HM pointing away from the charge, respectively (Fig. 1, A and B). Symmetrical arrangements of

charges cancel the HM, independent of the sign of these charges (Fig. 1, C, D, J, and M). Charges of opposite sign placed closely together (Fig. 1 F) compensate each other's effect to some extent, leading to a slightly smaller HM vector relative to that in the situation with charges of like sign (Fig. 1 E). HM vectors increase in length the more unbalanced is the distribution of polar and nonpolar surface areas (Fig. 1, B, E, and G). The effect of neighboring charges of opposite sign is described in more detail in Fig. 1, H and K. In Fig. 1 H, the vector is rotated slightly relative to that in Fig. 1 G, and in contrast to Fig. 1 J, where the HM is canceled, a small nonzero vector is found in Fig. 1 K. Reversing the sign of all charges does not influence the HM at all (compare Fig. 1, I and L, with Fig. 1, H and K, respectively). Finally, meaningful and comparable HM vectors can be obtained even in highly charged molecules of different total molecular charge (Fig. 1, N and O).

These examples show that the HM is a quantity independent of the total charge. It is similar in definition to the dipole moment, but is a different measure of the charge distribution. The vector represents the distribution of polar and nonpolar parts of a molecular surface, at the same time taking into account solvation effects and partial charge compensation via salt bridges. Since the distribution of nonpolar surface patches is crucial in many areas of macromolecular interactions—from protein oligomerization to receptor-ligand recognition and peptide-bilayer binding, the HM vector serves as a useful descriptor of macromolecular shape-dependent properties.
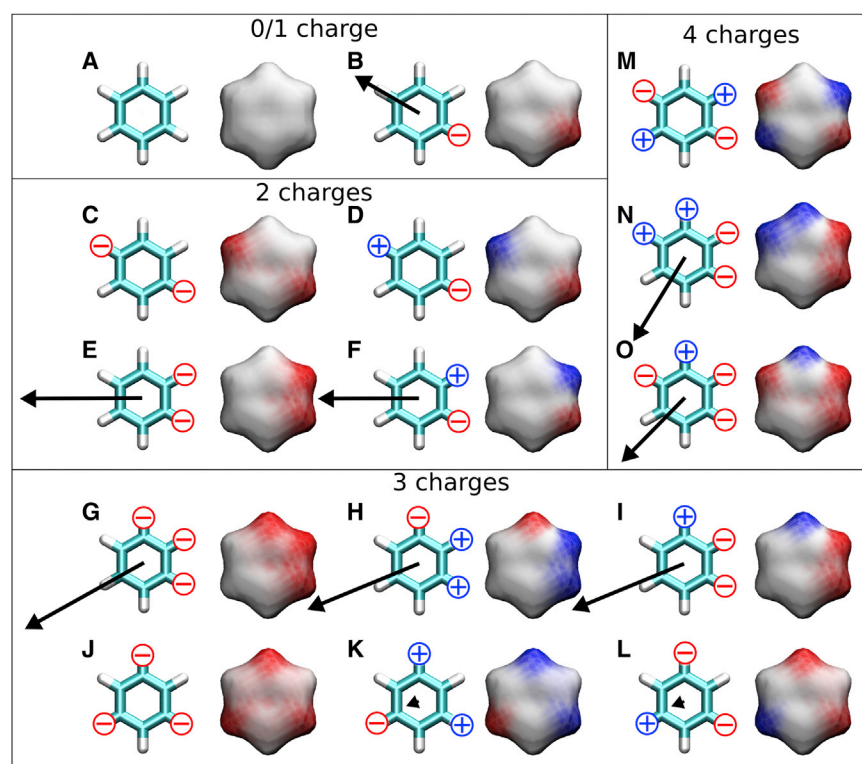

FIGURE 1   HM vectors and surface electrostatic potential for various model charge distributions on a hexagonal pseudomolecule. The HM vectors consistently point toward the most nonpolar parts of the molecular surface, independent of the sign of the individual charges or the total molecular charge. The length of the arrow reflects the size of the HM ($\vec{\mu} = 0$ in cases without an arrow). To see this figure in color, go online.

Peptide studies

We calculated the HM based on conformational ensembles from long MD simulations (several hundred nanoseconds) for two amphiphilic antimicrobial peptides. The β-pleated decapeptide gramicidin S (*cyclo*[PVOL-^{D}F]$_2$) has a charge of $+2$ and possesses an intrinsic C2 symmetry (48,49,80–82). The α-helical 21-mer PGLa (GMASKAGA IAGKIAKVALKAL-NH$_2$) has a charge of $+5$ due to its amidated C terminus (11,30,39,41,46,47,51,52,75–79).

Gramicidin S in solution

The cyclic antimicrobial peptide gramicidin S was simulated for 600 ns at 303 K, embedded in a cubic box of ~1000 methanol molecules (box side length ~4 nm). The peptide starting structure was obtained from high-resolution NMR data (87). All-atom RMSD evolution (see Fig. S1) shows that a minor structural rearrangement takes place after 130 ns simulation time, upon which a stable conformational ensemble is obtained. Fig. 2 gives the representative structure from a clustering analysis of the peptide, and the results of HM calculations based on the last 100 ns of the simulation data.

The HM vector is aligned almost perfectly with the molecular C2-symmetry axis, as expected, and it points away from the charged ornithine residues, passing between the hydrophobic side chains of the four valine and leucine residues. When all snapshots are aligned, the instantaneous HM vectors deviate from the time-averaged vector by $11° \pm 6°$, and the average length is expressed as 9.3 ± 0.9 (mean $\pm$ SD).

Gramicidin S in a membrane

Next, we calculated the HM for gramicidin S inserted into a lipid bilayer (see Fig. 3) for comparison with the results in isotropic solution (Fig. 2) and to see how the HM vector aligns with respect to the membrane normal. Here, the snapshots were taken from the last 100 ns of a 650 ns simulation in a bilayer composed of 72 preequilibrated DMPC molecules solvated with ~2000 TIP3P water molecules and chlo-
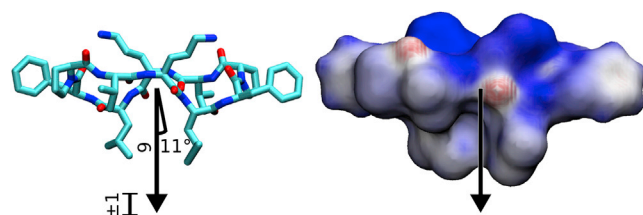

FIGURE 2 (*Left*) Representative structure of gramicidin S in methanol with its calculated HM vector. (*Right*) Electrostatic potential on the solvent-accessible surface of the same structure. The HM vector is pointing away from the surface region with high electrostatic potential. To see this figure in color, go online.

ride counterions. The RMSD evolution after the peptide is embedded in the membrane shows small conformational rearrangements up to ~250 ns of simulation time, after which a stable, converged structure is obtained (see Fig. S2). The peptide lies directly underneath the zwitterionic lipid headgroups, pointing its charged residues upward, toward the water. The distance between the center of mass of the heavy backbone atoms (N, C$_\alpha$, C, and O) of the peptide and the phosphorus atoms of the monolayer in which the peptide inserted was calculated from their average coordinates in the z-direction. To exclude data where the lipid position is influenced by the peptide, for each of the 36 lipids, only those time frames in which the distance to the peptide is >2.5 nm were included in the calculation. The last 400 ns were used to calculate the average values, which resulted in ~53,000 data points for the phosphorus atoms and ~8000 for the peptide. The peptide main chain lies 8.7 Å below the average phosphorus position. The standard deviation for the z-coordinate of the peptide is 1.4 Å, whereas the bilayer fluctuates more strongly, with a standard deviation of 2.2 Å. All three control simulations show a very similar average orientation upon insertion into the membrane. The resulting orientation of the peptide in the membrane is in full agreement with the results from solid-state NMR measurements of the C2-symmetry axis tilt angle and azimuthal rotation angle in an oriented DMPC sample with a peptide/lipid ratio of 1:80 (49).

The HM vector was calculated using an intermediate solvent dielectric constant of 20.0 to represent the conditions at the bilayer/water interface region. HM analysis shows that the fluctuations of the vector in this case are more pronounced than during the simulation in methanol, with an average angle variation of $18° \pm 10°$ and a standard deviation of the absolute length of ± 2.0 Å with respect to the average HM vector (Fig. 3).

Interestingly, the HM vector has increased significantly, by >50%, to 15.2 ± 2.0. This increase in length is caused partly by the smaller dielectric constant used in the Poisson-Boltzmann calculations (reducing solvent screening), but also by conformational changes of the peptide upon membrane binding. Exposing the molecule to a less polar environment leads to internal rearrangements that result in a more unequal distribution of polar and nonpolar surface residues. The charged ornithine side chains now point directly up into the solvent region, whereas the *D*-phenylalanine rings bend further down toward the hydrophobic bilayer core. Repeating the calculations of the HM vector with a dielectric constant of 32.6 yields an average HM vector length of 11.1, showing that structural rearrangements are responsible for ~30% of the difference in the HM vector lengths. The remaining 70% difference is due to the lower dielectric constant and less well screened electrostatic potential on the molecular surface. The resulting combined forces constrain the surface-bound geometry of gramicidin S in the membrane and lead to a lengthening
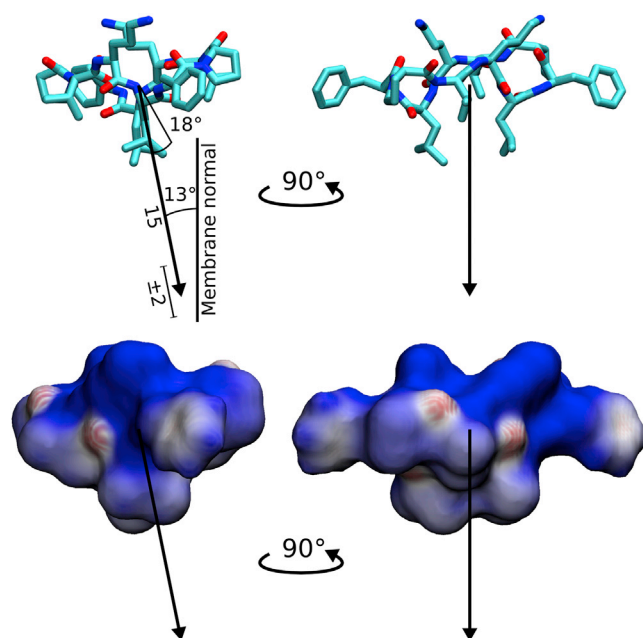
FIGURE 3 (*Upper*) Representative structure of gramicidin S embedded in a DMPC membrane (bilayer not shown; aligned horizontally) with its calculated HM vector. (*Lower*) Electrostatic potential on the solvent-accessible surface. The HM vector is almost parallel to the membrane normal (13°). To see this figure in color, go online.

of the HM vector. The angle between the HM vector of the time-averaged peptide structure and the membrane normal is small, with a value of only 13°, i.e., it points almost straight into the membrane core, as expected. For individual snapshots, the angle undergoes considerable fluctuation and measures on average 29° ± 17°, indicating that the small, surface-bound peptide behaves rather dynamically when embedded in the membrane. We also performed three control simulations, which gave similar results (see Table S2).

PGLa in a membrane

For peptides that retain a predominantly helical structure in their membrane-bound state, we can compare the 3D HM vector defined above with the conventional 2D HM. The antimicrobial peptide PGLa, which contains five positively charged residues along one face of the α-helix, was simulated for 600 ns at 303 K, embedded in a preequilibrated bilayer composed of 100 DMPC lipid molecules, solvated with ~3000 TIP3P water molecules and chloride counterions. The RMSD evolution of the surface-bound peptide shows a stable structure with no significant conformational changes after 200 ns simulation time (see Fig. S3). PGLa maintains a completely helical fold in the unrestrained simulation, in good agreement with the high helical content measured in CD experiments (47). The helix lies stably in the membrane-water interface. The insertion depth of the peptide was calculated as outlined in the previous section. For the linear PGLa molecule, we used average positions

of the centers of mass of the heavy backbone atoms (N, C_α, C, and O) for the C- and N-terminal residues and those of the 50 lipids that are >2.5 nm away from the peptide. The C terminus lies 10.8 Å below and the N-terminus only 5.3 Å below the average phosphorus layer. The standard deviations for the z-coordinates are 2.0 Å for the N terminus and 2.7 Å for the C terminus of PGLa, and 2.4 Å for the phosphorus atoms. All control simulations show a very similar average orientation upon insertion into the membrane. The peptide is pointing its charged lysine side chains up toward the water phase. The long axis is aligned flat on the membrane surface at an average tilt angle of 93° ± 7° with respect to the membrane normal. This alignment is very close to the experimentally obtained 95° determined by solid-state NMR in oriented DMPC bilayers at a peptide/lipid molar ratio of 1:200 (30,47,77,79).

The HM vector analysis was conducted over the last 100 ns of simulation time. The resulting HM vector and the corresponding electrostatic surface potential of the molecule are shown in Fig. 4.

The HM vector points away from the charged lysine residues, but the angle between the HM vector and the helix axis is only 39° ± 5°. This makes an important difference compared to the implicit value of 90° imposed by the conventional 2D HM analysis. Several factors contribute to the pronounced inclination of the vector toward the C terminus, including an unbalanced charge distribution along the peptide sequence, the additional charge at the uncapped N-terminus, and a large hydrophobic patch formed by a
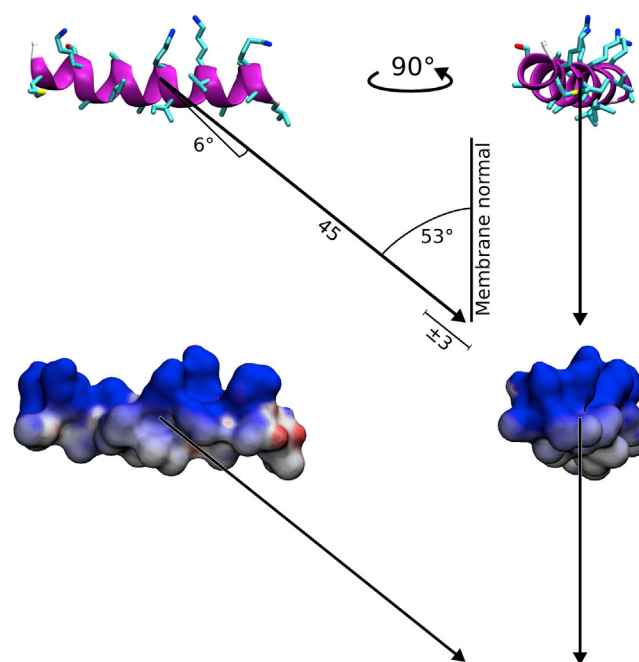

FIGURE 4 (*Upper*) Representative structure of PGLa in a DMPC membrane (bilayer not shown; aligned horizontally) with its calculated HM vector. (*Lower*) Electrostatic potential on the solvent-accessible surface. To see this figure in color, go online.

C-terminal leucine residue. At the same time, the HM vector of the time-averaged peptide structure is tilted quite far from the membrane normal, by 53°. When this angle is added to its tilt angle of 39° relative to the helix axis, the sum of 92° is consistent with a peptide helix aligned essentially perpendicular to the membrane normal, as described above and by solid-state NMR. The HM projection perpendicular to the helical axis aligns well with the membrane normal. The length of the vector is 44.9 ± 3.3, significantly larger than the value for gramicidin S, above, which indicates that PGLa is not only highly charged but has a very unequal polarity distribution along the helix. We also performed two control simulations, which gave very similar results (Table S2).

A comparison of the 3D HM vector obtained by our method with the original 2D HM definition by Eisenberg et al. (72) shows that the projection of the 3D HM vector onto the plane orthogonal to the helix axis results in closely aligned vectors (within an angle of 18°; see Fig. 5).

Notably, the new definition of the HM in 3D not only properly reproduces the unequal distribution of polar residues on the helical wheel of PGLa but also contains additional information about their distribution along the helix. Our HM calculations suggest that PGLa should have a tendency to insert its C terminus more deeply into the hydrophobic core than its N-terminus, such that the HM aligns more closely with the membrane normal. Such a strongly tilted peptide orientation is not seen in our simulations, probably due to sampling constraints. The membrane-bound geometry observed here corresponds to the so-called surface state obtained by solid-state NMR at a peptide/lipid ratio of 1:200 (30,47,77,79). However, a second, distinct membrane-bound structure has been found for PGLa in NMR experiments at a higher peptide/lipid ratio of 1:50 (30,47,77,79). In this so-called tilted state, the helix axis

is inclined at an angle of 127° with respect to the membrane normal. In this tilted orientation, our HM vector would be aligned almost parallel to the membrane normal (at 17°, as seen in Fig. 6).

It has been argued, based on the concentration dependence (47,77), and on MD analysis (1,62), that the tilted state of PGLa may be accompanied by dimerization. The peptide obviously experiences different forces and different stabilizing interactions under different conditions, and it will adjust its geometry in the membrane according to the dominant influence. We may thus suggest that the HM vector represents one of these factors and contributes strongly to stabilizing the strongly tilted membrane-bound structure of PGLa that has been observed experimentally.

PGLa in water

We showed above that for gramicidin S, the HM vector becomes longer when the peptide binds to a membrane. To check whether this holds also for PGLa, starting from an ideal helical structure, the peptide was simulated for 600 ns in a water box that included counterions. However, the peptide quickly unfolded in the polar medium and collapsed into a compact state resembling an unstructured coil (see RMSD plot in Fig. S4). Here, the polar regions tend to point toward the surrounding solvent, whereas the hydrophobic residues are packed into the core. The HM vector is drastically reduced in this conformation, by ~90%, to an average length of 5.5 ± 1.2 (see Fig. 7).

The HM calculation was performed both with a dielectric constant of 78.5 to represent water, and with a dielectric constant of 20.0, as above, to be able to distinguish
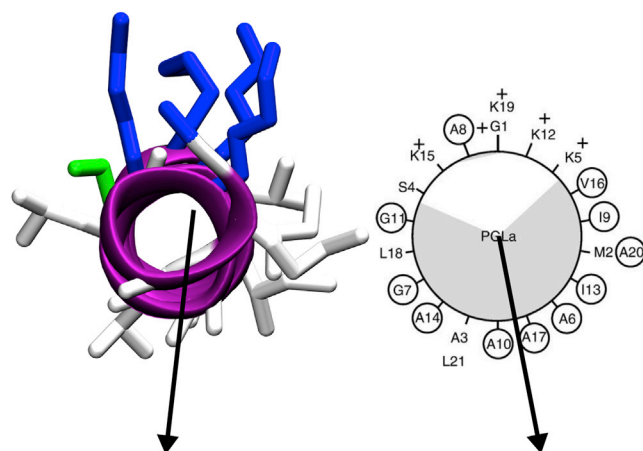

FIGURE 5 (*Left*) Projection of the 3D HM vector from this work onto the helix cross section of PGLa. (*Right*) Conventional 2D HM vector calculated according to Eisenberg (71). (The vectors have been normalized.) To see this figure in color, go online.
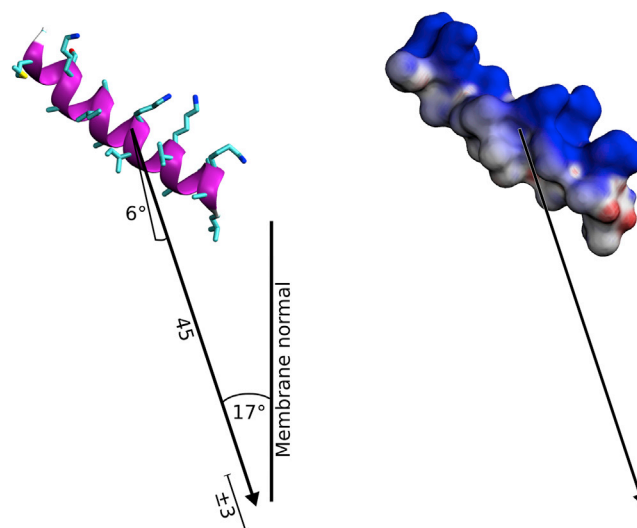

FIGURE 6 (*Left*) Tilted state of PGLa as measured experimentally by solid-state NMR in DMPC membranes at a peptide/lipid ratio of 1:50 (79) (bilayer not shown; aligned horizontally), shown with its HM vector calculated from MD simulations. (*Right*) Electrostatic potential on the solvent-accessible surface. To see this figure in color, go online.
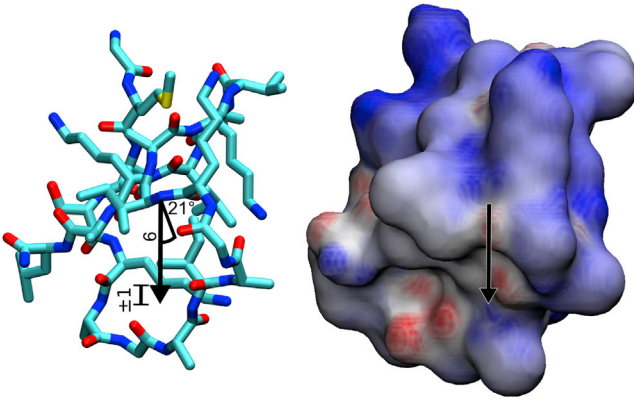
FIGURE 7 (*Left*) Representative structure of largely unfolded PGLa in water with its calculated HM vector. (*Right*) Electrostatic potential on the solvent-accessible surface. To see this figure in color, go online.

between the contribution of the different dielectric environment and that of the conformational change. We find that around two-thirds of the reduction of the HM can be attributed to the conformational change and one-third to the different dielectric constant used in the electrostatics calculations.

Results summary

The HM vector properties for the different systems investigated here are summarized in Table 1. We see that the time-dependent HM vector typically maintains a fairly constant length and orientation with respect to the peptide structure during any given simulation, but it can undergo considerable changes when the environmental conditions change, e.g., upon membrane embedding. The HM indicates a favorable orientation in which a peptide can bind to a lipid bilayer surface. However, the HM vector does not have to be aligned parallel with the membrane normal if the peptide in question contains an asymmetrical distribution of charged or nonpolar residues along its sequence, or if other forces dominate the geometry of peptide insertion.

DISCUSSION

The 3D HM vector as described in this work extends the classical 2D HM concept introduced by Eisenberg and co-workers in several ways. 1), It is applicable to arbitrary molecular structures, not only to regular conformations like α-helices or β-sheets. Individual side-chain rearrangements are taken into account as well as bent helices, partial unfolding, or unusual structures like the cyclic gramicidin S. 2), Charge compensation caused by salt bridges or hydrogen bond formation is reflected in the resulting electrostatic potential on the molecular surface. 3), In addition, it is possible to perform MD simulations to calculate the HM time average over a realistic ensemble of highly dynamical peptide structures in fluid membranes.

The results obtained for the HM vectors of gramicidin S in solution and when bound to a DMPC bilayer agree very well with both chemical intuition and experimental data. We find that the peptide rearranges its flexible side chains, resulting in an elongated HM vector in the membrane-bound state. For PGLa, the HM vector points into the membrane at an oblique angle in our simulations, due to the uneven arrangement of polar residues along the helix. Interestingly, the HM vector does not align with the membrane normal in this simulated orientation, but it would do so in another tilted alignment that has been experimentally observed at a different peptide/lipid ratio. We find that PGLa is not stable as a helix in aqueous solution, but it forms an amphiphilic helix upon binding to the membrane surface, in full agreement with experimental observations (47,96). This structural rearrangement produces a long HM vector only for the membrane-bound state.

The 3D HM vector is a useful tool for classifying the amphipathicity of peptides. It can predict which face of the peptide orients toward the membrane, even though it may not be sufficient to explain the exact alignment of the membrane-inserted monomer. There are several forces, and possibly competing contributions, that will determine the actual orientation of a peptide bound to a lipid bilayer.

TABLE 1   Summary of the HM vectors calculated for the last 100 ns of long MD simulations

System	Average HM vector length (kTÅ/e)[a]	Average angle deviation from average HM vector (°)[b]	Average angle between HM vector and membrane normal (°)[c]	Angle between average HM vector and membrane normal (°)[d]
Gramicidin S in methanol	9.3 ± 0.9	11.1 ± 5.9	—	—
Gramicidin S in membrane	15.2 ± 2.0	17.9 ± 9.5	28.8 ± 17.1	12.6
PGLa in water	5.5 ± 1.2	21.1 ± 13.0	—	—
PGLa in membrane	44.9 ± 3.3	5.7 ± 2.8	53.3 ± 6.6	53.2

Values are expressed as the mean ± SD.

[a]Average of the absolute values of all 100 vectors calculated from the snapshots.

[b]Average angular difference between each snapshot vector and the average vector when all snapshot conformations have been optimally aligned. The relatively high standard deviations relative to these values show that the single-frame vectors are not on a cone around the average vector (in which case they would have to be very small) but rather are spread.

[c]Average of the angle between the HM vector and the membrane normal in each snapshot.

[d]Angle between the average HM vector after all snapshots are aligned, and the membrane normal. For gramicidin S, it is remarkably different from the value in column 4. This shows that for the symmetrical gramicidin S, the HM vector is very flexible and averaging significantly decreases the single-frame angular values.

Regarding the HM vector, we expect that it has a stronger effect on shorter, and thus more globular, peptides (like gramicidin S) than on extended structures (like PGLa). Other, specific interactions between the lipid headgroups and peptide side chains, such as hydrogen bonds, could play a role in preventing the peptide from taking on a position in which the HM vector would be perfectly aligned with the membrane normal. Also, the overall dipole moment of the peptide (e.g., as intrinsically found along every helix axis) is of importance in determining the preferred geometry of insertion into charged as well as zwitterionic membranes. Furthermore, the spontaneous lipid curvature and bilayer thickness have been shown to have an effect on the orientation of inserted peptides (27,28,97–99).

SUPPORTING MATERIAL

Five figures and two tables are available at http://www.biophysj.org/biophysj/supplemental/S0006-3495(14)00405-6.

REFERENCES

1. Ulmschneider, J. P., J. C. Smith, …, E. Strandberg. 2012. Reorientation and dimerization of the membrane-bound antimicrobial peptide PGLa from microsecond all-atom MD simulations. *Biophys. J.* 103:472–482.

2. Özdirekcan, S., C. Etchebest, …, P. F. Fuchs. 2007. On the orientation of a designed transmembrane peptide: toward the right tilt angle? *J. Am. Chem. Soc.* 129:15174–15181.

3. Ulmschneider, J. P., J. P. F. Doux, …, M. B. Ulmschneider. 2009. Peptide partitioning and folding into lipid bilayers. *J. Chem. Theory Comput.* 5:2202–2205.

4. Wang, Y., D. E. Schlamadinger, …, J. A. McCammon. 2012. Comparative molecular dynamics simulations of the antimicrobial peptide CM15 in model lipid bilayers. *Biochim. Biophys. Acta.* 1818:1402–1409.

5. Toraya, S., N. Javkhlantugs, …, A. Naito. 2010. Dynamic structure of bombolitin II bound to lipid bilayers as revealed by solid-state NMR and molecular-dynamics simulation. *Biophys. J.* 99:3282–3289.

6. Kandasamy, S. K., and R. G. Larson. 2006. Effect of salt on the interactions of antimicrobial peptides with zwitterionic lipid bilayers. *Biochim. Biophys. Acta.* 1758:1274–1284.

7. Kagan, B. L., H. Jang, …, R. Nussinov. 2012. Antimicrobial properties of amyloid peptides. *Mol. Pharm.* 9:708–717.

8. Mihajlovic, M., and T. Lazaridis. 2010. Antimicrobial peptides bind more strongly to membrane pores. *Biochim. Biophys. Acta.* 1798:1494–1502.

9. Ulmschneider, M. B., J. P. Doux, …, J. P. Ulmschneider. 2010. Mechanism and kinetics of peptide partitioning into membranes from all-atom simulations of thermostable peptides. *J. Am. Chem. Soc.* 132:3452–3460.

10. Hartmann, M., M. Berditsch, …, A. S. Ulrich. 2010. Damage of the bacterial cell envelope by antimicrobial peptides gramicidin S and PGLa as revealed by transmission and scanning electron microscopy. *Antimicrob. Agents Chemother.* 54:3132–3142.

11. Tremouilhac, P., E. Strandberg, …, A. S. Ulrich. 2006. Synergistic transmembrane alignment of the antimicrobial heterodimer PGLa/magainin. *J. Biol. Chem.* 281:32089–32094.

12. Alves, C. S., M. N. Melo, …, M. A. Castanho. 2010. *Escherichia coli* cell surface perturbation and disruption induced by antimicrobial peptides BP100 and pepR. *J. Biol. Chem.* 285:27536–27544.

13. Grage, S. L., S. Afonin, and A. S. Ulrich. 2010. Dynamic transitions of membrane-active peptides. *Methods Mol. Biol.* 618:183–207.

14. Esteban-Martín, S., E. Strandberg, …, A. S. Ulrich. 2010. Solid state NMR analysis of peptides in membranes: influence of dynamics and labeling scheme. *Biochim. Biophys. Acta.* 1798:252–257.

15. Strandberg, E., S. Esteban-Martín, …, A. S. Ulrich. 2009. Orientation and dynamics of peptides in membranes calculated from ^{2}H-NMR data. *Biophys. J.* 96:3223–3232.

16. Esteban-Martín, S., E. Strandberg, …, J. Salgado. 2009. Influence of whole-body dynamics on ^{15}N PISEMA NMR spectra of membrane proteins: a theoretical analysis. *Biophys. J.* 96:3233–3241.

17. Strandberg, E., S. Özdirekcan, …, J. A. Killian. 2004. Tilt angles of transmembrane model peptides in oriented and non-oriented lipid bilayers as determined by ^{2}H solid-state NMR. *Biophys. J.* 86:3709–3721.

18. van der Wel, P. C., E. Strandberg, …, R. E. Koeppe, 2nd. 2002. Geometry and intrinsic tilt of a tryptophan-anchored transmembrane α-helix determined by ^{2}H NMR. *Biophys. J.* 83:1479–1488.

19. Ulrich, A. S. 2005. Solid state ^{19}F-NMR methods for studying biomembranes. *Prog. Nucl. Magn. Reson. Spectrosc.* 46:1–21.

20. Strandberg, E., and A. S. Ulrich. 2004. NMR methods for studying membrane-active antimicrobial peptides. *Concepts Magn. Reson. Part A.* 23A:89–120.

21. Ulrich, A. S. 2006. Solid state ^{19}F-NMR analysis of oriented biomembranes. *In* Modern Magnetic Resonance. G. A. Webb, editor. Springer, Dordrecht, The Netherlands, pp. 261–267.

22. Wadhwani, P., and E. Strandberg. 2009. Structure analysis of membrane-active peptides using ^{19}F-labeled amino acids and solid-state NMR. *In* Fluorine in Medicinal Chemistry and Chemical Biology. I. Ojima, editor. Blackwell, London, pp. 463–493.

23. Gehman, J. D., and F. Separovic. 2006. Solid-state NMR of membrane-active proteins and peptides. *In* Modern Magnetic Resonance. G. A. Webb, editor. Springer, Dordrecht, The Netherlands, pp. 305–311.

24. Özdirekcan, S., D. T. S. Rijkers, …, J. A. Killian. 2005. Influence of flanking residues on tilt and rotation angles of transmembrane peptides in lipid bilayers. A solid-state ^{2}H NMR study. *Biochemistry.* 44:1004–1012.

25. Gleason, N. J., V. V. Vostrikov, …, R. E. Koeppe, 2nd. 2013. Buried lysine, but not arginine, titrates and alters transmembrane helix tilt. *Proc. Natl. Acad. Sci. USA.* 110:1692–1695.

26. Vostrikov, V. V., A. E. Daily, …, R. E. Koeppe, 2nd. 2010. Charged or aromatic anchor residue dependence of transmembrane peptide tilt. *J. Biol. Chem.* 285:31723–31730.

27. Strandberg, E., D. Tiltak, …, A. S. Ulrich. 2012. Lipid shape is a key factor for membrane interactions of amphipathic helical peptides. *Biochim. Biophys. Acta.* 1818:1764–1776.

28. Strandberg, E., S. Esteban-Martín, …, J. Salgado. 2012. Hydrophobic mismatch of mobile transmembrane helices: merging theory and experiments. *Biochim. Biophys. Acta.* 1818:1242–1249.

29. Strandberg, E., N. Kanithasen, …, A. S. Ulrich. 2008. Solid-state NMR analysis comparing the designer-made antibiotic MSI-103 with its parent peptide PGLa in lipid bilayers. *Biochemistry.* 47:2601–2616.

30. Strandberg, E., P. Wadhwani, …, A. S. Ulrich. 2006. Solid-state NMR analysis of the PGLa peptide orientation in DMPC bilayers: structural fidelity of ^{2}H-labels versus high sensitivity of ^{19}F-NMR. *Biophys. J.* 90:1676–1686.

31. Bechinger, B., Y. Kim, …, S. J. Opella. 1991. Orientations of amphipathic helical peptides in membrane bilayers determined by solid-state NMR spectroscopy. *J. Biomol. NMR.* 1:167–173.

32. Ramamoorthy, A., Y. F. Wei, and D. K. Lee. 2004. PISEMA solid-state NMR spectroscopy. *Annu. Rep. NMR Spectrosc.* 52:1–52.

33. Denny, J. K., J. F. Wang, …, J. R. Quine. 2001. PISEMA powder patterns and PISA wheels. *J. Magn. Reson.* 152:217–226.

34. Balla, M. S., J. H. Bowie, and F. Separovic. 2004. Solid-state NMR study of antimicrobial peptides from Australian frogs in phospholipid membranes. *Eur. Biophys. J.* 33:109–116.

35. Grage, S. L., E. Strandberg, …, A. S. Ulrich. 2012. Comparative analysis of the orientation of transmembrane peptides using solid-state ^{2}H- and ^{15}N-NMR: mobility matters. *Eur. Biophys. J.* 41:475–482.

36. Walther, T. H., S. L. Grage, …, A. S. Ulrich. 2010. Membrane alignment of the pore-forming component TatA$_d$ of the twin-arginine translocase from *Bacillus subtilis* resolved by solid-state NMR spectroscopy. *J. Am. Chem. Soc.* 132:15945–15956.

37. Koch, K., S. Afonin, …, A. S. Ulrich. 2012. Solid-state ^{19}F-NMR of peptides in native membranes. *Top. Curr. Chem.* 306:89–118.

38. Wadhwani, P., E. Strandberg, …, A. S. Ulrich. 2012. Self-assembly of flexible β-strands into immobile amyloid-like β-sheets in membranes as revealed by solid-state ^{19}F NMR. *J. Am. Chem. Soc.* 134:6512–6515.

39. Ieronimo, M., S. Afonin, …, A. S. Ulrich. 2010. ^{19}F NMR analysis of the antimicrobial peptide PGLa bound to native cell membranes from bacterial protoplasts and human erythrocytes. *J. Am. Chem. Soc.* 132:8822–8824.

40. Maisch, D., P. Wadhwani, …, A. S. Ulrich. 2009. Chemical labeling strategy with (R)- and (S)-trifluoromethylalanine for solid state ^{19}F NMR analysis of peptaibols in membranes. *J. Am. Chem. Soc.* 131:15596–15597.

41. Afonin, S., S. L. Grage, …, A. S. Ulrich. 2008. Temperature-dependent transmembrane insertion of the amphiphilic peptide PGLa in lipid bilayers observed by solid state ^{19}F NMR spectroscopy. *J. Am. Chem. Soc.* 130:16512–16514.

42. Wadhwani, P., J. Bürck, …, A. S. Ulrich. 2008. Using a sterically restrictive amino acid as a ^{19}F NMR label to monitor and to control peptide aggregation in membranes. *J. Am. Chem. Soc.* 130:16515–16517.

43. Dürr, U. H. N., S. L. Grage, …, A. S. Ulrich. 2008. Solid state ^{19}F NMR parameters of fluorine-labeled amino acids. Part I: Aromatic substituents. *J. Magn. Reson.* 191:7–15.

44. Grage, S. L., U. H. N. Dürr, …, A. S. Ulrich. 2008. Solid state ^{19}F NMR parameters of fluorine-labeled amino acids. Part II: Aliphatic substituents. *J. Magn. Reson.* 191:16–23.

45. Witter, R., F. Nozirov, …, R. Fu. 2008. Solid-state ^{19}F NMR spectroscopy reveals that Trp^{41} participates in the gating mechanism of the M2 proton channel of influenza A virus. *J. Am. Chem. Soc.* 130:918–924.

46. Glaser, R. W., C. Sachse, …, A. S. Ulrich. 2005. Concentration-dependent realignment of the antimicrobial peptide PGLa in lipid membranes observed by solid-state ^{19}F-NMR. *Biophys. J.* 88:3392–3397.

47. Glaser, R. W., C. Sachse, …, A. S. Ulrich. 2004. Orientation of the antimicrobial peptide PGLa in lipid membranes determined from ^{19}F-NMR dipolar couplings of 4-CF$_3$-phenylglycine labels. *J. Magn. Reson.* 168:153–163.

48. Salgado, J., S. L. Grage, …, A. S. Ulrich. 2001. Membrane-bound structure and alignment of the antimicrobial β-sheet peptide gramicidin S derived from angular and distance constraints by solid state ^{19}F-NMR. *J. Biomol. NMR.* 21:191–208.

49. Afonin, S., U. H. N. Dürr, …, A. S. Ulrich. 2008. Solid state NMR structure analysis of the antimicrobial peptide gramicidin S in lipid membranes: concentration-dependent re-alignment and self-assembly as a β-barrel. *Top. Curr. Chem.* 273:139–154.

50. Afonin, S., U. H. N. Dürr, …, A. S. Ulrich. 2004. "Boomerang"-like insertion of a fusogenic peptide in a lipid membrane revealed by solid-state ^{19}F NMR. *Magn. Reson. Chem.* 42:195–203.

51. Afonin, S., P. K. Mikhailiuk, …, A. S. Ulrich. 2007. Evaluating the amino acid CF$_3$-bicyclopentylglycine as a new label for solid-state ^{19}F-NMR structure analysis of membrane-bound peptides. *J. Pept. Sci.* 13:614–623.

52. Bürck, J., S. Roth, …, A. S. Ulrich. 2008. Conformation and membrane orientation of amphiphilic helical peptides by oriented circular dichroism. *Biophys. J.* 95:3872–3881.

53. Olah, G. A., and H. W. Huang. 1988. Circular dichroism of oriented α-helices. II. Electric field oriented polypeptides. *J. Chem. Phys.* 89:6956–6962.

54. Olah, G. A., and H. W. Huang. 1988. Circular dichroism of oriented α-helices. I. Proof of the exciton theory. *J. Chem. Phys.* 89:2531–2538.

55. Wu, Y., H. W. Huang, and G. A. Olah. 1990. Method of oriented circular dichroism. *Biophys. J.* 57:797–806.

56. Nolandt, O. V., T. H. Walther, …, A. S. Ulrich. 2009. Structure analysis of the membrane protein TatC(d) from the Tat system of *B. subtilis* by circular dichroism. *Biochim. Biophys. Acta.* 1788:2238–2244.

57. Heinzmann, R., S. L. Grage, …, A. S. Ulrich. 2011. A kinked antimicrobial peptide from *Bombina maxima*. II. Behavior in phospholipid bilayers. *Eur. Biophys. J.* 40:463–470.

58. Steinbrecher, T., S. Prock, …, A. S. Ulrich. 2012. Peptide-lipid interactions of the stress-response peptide TisB that induces bacterial persistence. *Biophys. J.* 103:1460–1469.

59. Monticelli, L., S. K. Kandasamy, …, S. J. Marrink. 2008. The MARTINI coarse-grained force field: extension to proteins. *J. Chem. Theory Comput.* 4:819–834.

60. Hsu, J. C., and C. M. Yip. 2007. Molecular dynamics simulations of indolicidin association with model lipid bilayers. *Biophys. J.* 92:L100–L102.

61. Esteban-Martín, S., and J. Salgado. 2007. The dynamic orientation of membrane-bound peptides: bridging simulations and experiments. *Biophys. J.* 93:4278–4288.

62. Wang, Y., T. Zhao, D. Wei, A. S. Ulrich, E. Strandberg, and J. P. Ulmschneider. 2014. How reliable are molecular dynamics simulations of membrane active antimicrobial peptides? *Biochim. Biophys. Acta.* In press. http://dx.doi.org/10.1016/j.bbamem.2014.04.009.

63. Du, Q., P. G. Mezey, and K. C. Chou. 2005. Heuristic molecular lipophilicity potential (HMLP): a 2D-QSAR study to LADH of molecular family pyrazole and derivatives. *J. Comput. Chem.* 26:461–470.

64. Efremov, R. G., A. O. Chugunov, …, E. Jacoby. 2007. Molecular lipophilicity in protein modeling and drug design. *Curr. Med. Chem.* 14:393–415.

65. Wimley, W. C., and S. H. White. 1996. Experimentally determined hydrophobicity scale for proteins at membrane interfaces. *Nat. Struct. Biol.* 3:842–848.

66. Wimley, W. C., T. P. Creamer, and S. H. White. 1996. Solvation energies of amino acid side chains and backbone in a family of host-guest pentapeptides. *Biochemistry.* 35:5109–5124.

67. Engelman, D. M., T. A. Steitz, and A. Goldman. 1986. Identifying nonpolar transbilayer helices in amino acid sequences of membrane proteins. *Annu. Rev. Biophys. Biophys. Chem.* 15:321–353.

68. Kyte, J., and R. F. Doolittle. 1982. A simple method for displaying the hydropathic character of a protein. *J. Mol. Biol.* 157:105–132.

69. Wildman, S. A., and G. M. Crippen. 1999. Prediction of physicochemical parameters by atomic contributions. *J. Chem. Inf. Comput. Sci.* 39:868–873.

70. Snider, C., S. Jayasinghe, …, S. H. White. 2009. MPEx: a tool for exploring membrane proteins. *Protein Sci.* 18:2624–2628.

71. Eisenberg, D., R. M. Weiss, and T. C. Terwilliger. 1982. The helical hydrophobic moment: a measure of the amphiphilicity of a helix. *Nature.* 299:371–374.

72. Eisenberg, D., R. M. Weiss, …, W. Wilcox. 1982. Hydrophobic moments and protein structure. *Faraday Sym.p Chem. Soc.* 17:109–120.

73. Beuming, T., and H. Weinstein. 2004. A knowledge-based scale for the analysis and prediction of buried and exposed faces of transmembrane domain proteins. *Bioinformatics.* 20:1822–1835.

74. Vik, S. B. 2011. The transmembrane helices of the L, M, and N subunits of Complex I from *E. coli* can be assigned on the basis of conservation and hydrophobic moment analysis. *FEBS Lett.* 585:1180–1184.

75. Soravia, E., G. Martini, and M. Zasloff. 1988. Antimicrobial properties of peptides from *Xenopus* granular gland secretions. *FEBS Lett.* 228:337–340.

76. Bechinger, B., M. Zasloff, and S. J. Opella. 1998. Structure and dynamics of the antibiotic peptide PGLa in membranes by solution and solid-state nuclear magnetic resonance spectroscopy. *Biophys. J.* 74:981–987.

77. Tremouilhac, P., E. Strandberg, …, A. S. Ulrich. 2006. Conditions affecting the re-alignment of the antimicrobial peptide PGLa in membranes as monitored by solid state ^{2}H-NMR. *Biochim. Biophys. Acta.* 1758:1330–1342.

78. Strandberg, E., D. Tiltak, …, A. S. Ulrich. 2007. Influence of C-terminal amidation on the antimicrobial and hemolytic activities of cationic α-helical peptides. *Pure Appl. Chem.* 79:717–728.

79. Strandberg, E., P. Tremouilhac, …, A. S. Ulrich. 2009. Synergistic transmembrane insertion of the heterodimeric PGLa/magainin 2 complex studied by solid-state NMR. *Biochim. Biophys. Acta.* 1788:1667–1679.

80. Gause, G. G., and M. G. Brazhnikova. 1944. Gramicidin S and its use in the treatment of infected wounds. *Nature.* 154:703.

81. Gause, G. F., and M. G. Brazhnikova. 1944. Gramicidin S. Origin and mode of action. *Lancet.* 247:715–716.

82. Grage, S. L., A. V. Suleymanova, …, A. S. Ulrich. 2006. Solid state NMR analysis of the dipolar couplings within and between distant CF_3-groups in a membrane-bound peptide. *J. Magn. Reson.* 183:77–86.

83. Pronk, S., S. Páll, …, E. Lindahl. 2013. GROMACS 4.5: a high-throughput and highly parallel open source molecular simulation toolkit. *Bioinformatics.* 29:845–854.

84. Lindorff-Larsen, K., S. Piana, …, D. E. Shaw. 2010. Improved side-chain torsion potentials for the Amber ff99SB protein force field. *Proteins.* 78:1950–1958.

85. Jämbeck, J. P. M., and A. P. Lyubartsev. 2012. Derivation and systematic validation of a refined all-atom force field for phosphatidylcholine lipids. *J. Phys. Chem. B.* 116:3164–3179.

86. Case, D. A., T. A. Darden, …, P. A. Kollman. 2012. AMBER 12. University of California, San Francisco.

87. Xu, Y., I. P. Sugár, and N. R. Krishna. 1995. A variable target intensity-restrained global optimization (VARTIGO) procedure for determining three-dimensional structures of polypeptides from NOESY data: application to gramicidin-S. *J. Biomol. NMR.* 5:37–48.

88. Nosé, S. 1984. A molecular dynamics method for simulations in the canonical ensemble. *Mol. Phys.* 52:255–268.

89. Parrinello, M., and A. Rahman. 1981. Polymorphic transitions in single crystals: a new molecular dynamics method. *J. Appl. Phys.* 52:7182–7190.

90. Hess, B., H. Bekker, …, J. G. E. M. Fraaije. 1997. LINCS: A linear constraint solver for molecular simulations. *J. Comput. Chem.* 18:1463–1472.

91. Sitkoff, D., K. A. Sharp, and B. Honig. 1994. Accurate calculation of hydration free energies using macroscopic solvent models. *J. Phys. Chem.* 98:1978–1988.

92. Decherchi, S., and W. Rocchia. 2013. A general and robust ray-casting-based algorithm for triangulating surfaces at the nanoscale. *PLoS ONE.* 8:e59744.

93. Baker, N. A., D. Sept, …, J. A. McCammon. 2001. Electrostatics of nanosystems: application to microtubules and the ribosome. *Proc. Natl. Acad. Sci. USA.* 98:10037–10041.

94. Humphrey, W., A. Dalke, and K. Schulten. 1996. VMD: visual molecular dynamics. *J. Mol. Graph.* 14:33–38, 27–28.

95. Reference deleted in proof.

96. Latal, A., G. Degovics, …, K. Lohner. 1997. Structural aspects of the interaction of peptidyl-glycylleucine-carboxyamide, a highly potent antimicrobial peptide from frog skin, with lipids. *Eur. J. Biochem.* 248:938–946.

97. Muhle-Goll, C., S. Hoffmann, …, A. S. Ulrich. 2012. Hydrophobic matching controls the tilt and stability of the dimeric platelet-derived growth factor receptor (PDGFR) β transmembrane segment. *J. Biol. Chem.* 287:26178–26186.

98. Strandberg, E., J. Zerweck, …, A. S. Ulrich. 2013. Synergistic insertion of antimicrobial magainin-family peptides in membranes depends on the lipid spontaneous curvature. *Biophys. J.* 104:L9–L11.

99. Afonin, S. E., R. W. Glaser, …, A. S. Ulrich. 2014. ^{19}F-NMR screening of unrelated antimicrobial peptides shows that membrane interactions are governed by lipids. *Biochim. Biophys. Acta.* In press. http://dx.doi.org/10.1016/j.bbamem.2014.03.017.